Polymer Bulletin (2026) 83:500
https://doi.org/10.1007/s00289-026-06566-4

ORIGINAL PAPER

Alternan exopolysaccharide as a novel precursor for hydrogel and cryogel wound dressings

Sanem Bulut[1] · Semra Tasdurmazli[2] · Esra Bedir[2] · Tulin Ozbek[2] · Esra Su[3] · Kader Korkmaz Edis[4] · Enes Dertli[5] · Mehmet Murat Ozmen[1]

Received: 17 March 2026 / Revised: 9 June 2026 / Accepted: 19 June 2026
© The Author(s) 2026

Abstract

The development of wound dressings that effectively manage exudate while providing antibacterial protection remains a key challenge. Cryogels offer advantages over conventional hydrogels due to their macroporous structure; however, while numerous biopolymer precursors have been employed in the synthesis of such materials, identifying sustainable and renewable alternatives remains of significant interest. In this context, alternan exopolysaccharide extracted from *Limosilactobacillus reuteri* E81 was cross-linked with epichlorohydrin to form hydrogels at 20 °C and cryogels at -20 °C. The cryogels exhibited a highly interconnected macroporous structure with an average pore size in the range of 84 ± 31 µm and a swelling equilibrium ratio q_w of 14.01 ± 0.19. While cryogels reached equilibrium swelling in less than a minute due to their highly interconnected macroporous structure, mechanical testing demonstrated that cryogels possessed increased flexibility and withstood compressive stresses up to 12 MPa in the dry state. Vancomycin was subsequently loaded into the cryogels, and the resulting vancomycin-loaded cryogels effectively inhibited *Staphylococcus aureus* strains exhibiting different resistance profiles. Also, bioavailability and in vitro wound healing analyses demonstrated that vancomycin incorporation did not compromise cellular compatibility, while the vancomycin loaded cryogel samples exhibited higher cell viability at 24 h and enhanced fibroblast migration compared to unloaded samples, indicating a favorable cytocompatibility and wound closure profile. These findings underscore that alternan-based cryogels constitute a promising antibacterial wound-dressing platform, while also illustrating the broader potential of alternan as a novel and versatile biopolymer for gel fabrication and wound healing applications.

Extended author information available on the last page of the article

Published online: 26 June 2026

Graphical abstract

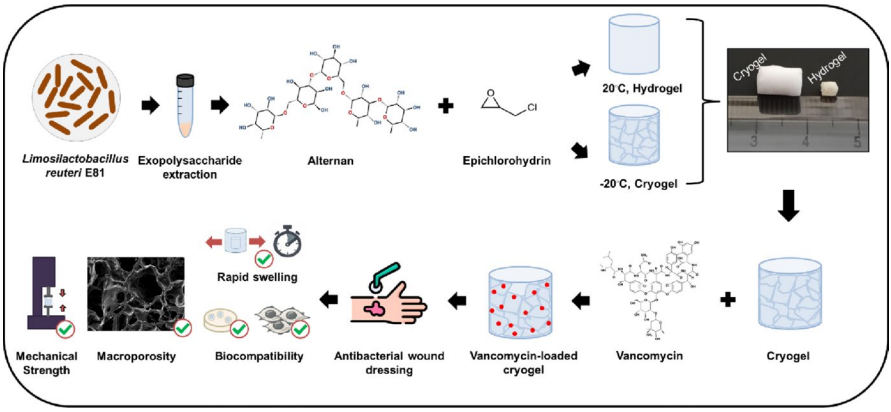

Keywords Alternan · Antibacterial · Cryogel · Exopolysaccharide · Hydrogel · Wound dressing

Introduction

The development of effective wound dressing materials remains a major challenge in biomaterials research, as an ideal dressing must simultaneously manage wound exudate, maintain a moist healing environment, conform to irregular tissue surfaces, and prevent bacterial infection [1]. Polymeric hydrogels have long been explored for such applications because their three-dimensional, crosslinked networks can absorb and retain large amounts of water while remaining insoluble in aqueous environments [2]. Their soft and elastic nature enables close contact with tissue, making them attractive for wound care, tissue engineering, and drug delivery systems. However, conventional hydrogels often suffer from insufficient mechanical robustness and slow swelling [3].

To overcome these limitations, increasing attention has been directed toward macroporous hydrogels, so-called cryogels. Cryogels represent a distinct class of hydrogels formed via cryogelation, in which ice crystals act as porogens during crosslinking at sub-zero temperatures. Crosslinking reactions occur in the unfrozen microphase surrounding the ice crystals, and subsequent thawing results in a highly interconnected macroporous network [4, 5]. This macroporous structure enables cryogels to swell rapidly, support fluid transport, and recover their shape after deformation which are features that are highly desirable in wound dressings where excess exudate must be managed efficiently [6–9]. Beyond swelling behavior, an ideal dressing must also ensure biocompatibility, maintain a moist environment for healing, and remain flexible enough to conform to irregular wound surfaces. Importantly, it should help prevent bacterial colonization and infection, which remain major complications in clinical wound care [10]. While conventional hydrogels offer some of these benefits, their low swelling rate and weak mechanical properties limit their applications [11,

12]. Cryogels, with their macroporosity and improved resilience, represent a more promising option for advanced wound management applications [3].

The choice of polymer is a critical factor in determining the performance of hydrogel and cryogel materials. In recent years, the demand for sustainable, renewable, and bio-based polymers has increased, driving interest toward alternative natural polymers. Among these, microbial exopolysaccharides (EPSs) have emerged as particularly attractive candidates due to their biodegradability, biocompatibility, and structural diversity [13]. EPSs are carbohydrate-based biopolymers secreted by microorganisms into their extracellular environment [14]. Their molecular structures contain numerous functional groups, enabling versatile crosslinking strategies and allowing the fabrication of polymer networks with tunable swelling, mechanical, and transport properties [15].

While interest in EPS-based hydrogels has grown in recent years, most reported systems are still based on a limited group of widely used polysaccharides [16]. At the same time, microbial α-glucans produced by lactic acid bacteria remain relatively underexplored from a biomaterials perspective [17]. These α-glucans are produced by glucansucrase enzymes, and variations in their glycosidic linkage patterns among different microorganisms lead to differences in chain conformation and physicochemical properties [18, 19]. Recent studies highlight that the nature and distribution of these linkages strongly affect solubility, hydration, and intermolecular interactions, all of which are important for gel formation and function [20].

Alternan is a homopolysaccharide belonging to the α-D-glucan family and stands out because of its distinctive molecular structure. Unlike more commonly studied α-glucans, which are defined by a single type of glycosidic linkage such as dextran dominated by α-(1→6) bonds or mutan rich in α-(1→3) linkages, alternan contains an alternating α-(1→3)/α-(1→6) backbone [18, 21]. This mixed-linkage structure leads to differences in chain conformation and intermolecular organization compared to conventional α-glucans. As a result, alternan has been reported to exhibit high water solubility and low solution viscosity, as well as favorable film-forming behavior [22]. These features distinguish alternan from more traditional EPSs and suggest that it may offer distinct advantages as a promising structural polymer.

To date, research on alternan has focused on its microbial production, enzymatic synthesis, and characterization, as well as its potential applications in the food industry, including use as a low-glycemic sweetener, thickener, and prebiotic [18, 23]. More recent studies have started to reveal additional functional properties of alternan, such as its ability to form transparent films and nanostructures, and its compatibility with mammalian cells, suggesting potential for biomedical applications [22]. Despite these promising findings, to the best of our knowledge, alternan has not received any attention as a precursor for hydrogel and cryogel formation. In particular, its use as a matrix-forming biopolymer in wound dressing systems has not yet been reported. The combination of high water solubility, open-chain conformation arising from its alternating glycosidic linkages, film-forming ability, and biocompatibility positions alternan as a promising candidate for advanced wound dressing materials. Specifically, these properties may support cryogel network formation, promote exudate absorption, help maintain a moist wound environment, and contribute to tissue compatibility, all of which are desirable for effective wound management.

From a wound care perspective, the incorporation of antibacterial functionality into the dressing material is of critical importance. Hydrogel-based systems have been extensively investigated for the local delivery of antibiotics, as they allow high drug concentrations to be achieved at the target site while reducing systemic side effects [24]. Vancomycin, a glycopeptide antibiotic effective against Gram-positive bacteria including resistant *Staphylococcus aureus* strains, is frequently used in wound treatment strategies. Combining vancomycin with a gel matrix offers the potential to couple rapid fluid absorption with efficient drug diffusion, thereby addressing both exudate management and infection control [25]. The macroporous structure of cryogels may further facilitate rapid swelling and early drug availability at the wound site, which is advantageous during the initial stages of healing.

Although exopolysaccharide (EPS)-based hydrogels and cryogels have been investigated, and alternan has been recognized as a structurally unique α-glucan, its use in hydrogel and cryogel systems has not yet been reported. In this study, we address this gap by developing hydrogel and cryogel biomaterials derived from the α-D-glucan exopolysaccharide alternan. Alternan was extracted from *Limosilactobacillus reuteri* E81 and cross-linked with epichlorohydrin (ECH) to form both conventional hydrogels and macroporous cryogels. Furthermore, vancomycin-loaded alternan cryogels were prepared to introduce antibacterial functionality while preserving the cryogel network's favorable swelling and mechanical properties. The structural, morphological, swelling, mechanical, antibacterial, and biocompatibility properties of these materials were investigated to evaluate their potential as antibacterial wound dressings.

Experimental

Materials

Alternan was extracted from *Limosilactobacillus reuteri* E81 [18]. ECH (Fluka), sodium hydroxide (NaOH, Sigma-Aldrich), and vancomycin hydrochloride (Sigma-Aldrich), meat extract (Neogen), peptone casein (Neogen), sodium acetate trihydrate (Merck), Tween 80 (Merck), magnesium sulfate heptahydrate (Merck), and sucrose (BioShop) were used as received. *Staphylococcus aureus* (ATCC 25923) and OSSA (oxacillin-sensitive *S. aureus*), MORSA (methicillin/oxacillin-resistant *S. aureus*), MRSA (methicillin-resistant *S. aureus*), MSSA (methicillin-sensitive *S. aureus*) were acquired from the Microbiology Laboratory at the Department of Molecular Biology and Genetics, Yıldız Technical University.

Alternan extraction

For alternan extraction, the previously established methodology described by Dertli et al. was followed [26]. Briefly, *L. reuteri* E81, as an alternan producer strain, was cultured and incubated at 37 °C for 24 h in Brain Heart Infusion medium supplemented with meat extract, peptone casein, sodium acetate, Tween 80, magnesium sulfate heptahydrate, and sucrose. Following incubation, the bacterial suspension

was centrifuged at 10,300 rpm for 20 min at 4 °C to collect the supernatant. An equal volume of ethanol was added to the supernatant, and was incubated overnight at 4 °C. After the overnight incubation, the mixture was centrifuged again under the same conditions, and the resulting pellet was collected, dissolved in water, and re-precipitated by adding two volumes of ethanol, followed by another overnight incubation at 4 °C. After a final centrifugation, the pellet was dissolved in water, stored at -20 °C, and lyophilized to obtain alternan.

Gel synthesis

Alternan-based gels were synthesized via alkaline activation followed by ECH crosslinking. Briefly, 0.3 g of alternan was dissolved in 1.5 mL of 2.8 M NaOH and stirred for 60 min. 0.13 mL of ECH was then introduced as the crosslinking agent, and the reaction mixture was homogenized for 5 min before being transferred into 1 mL syringes.

To obtain alternan hydrogels (Alt-H), the filled syringes were maintained at 20 °C for 24 h, whereas cryogels (Alt-C) were prepared by incubating the syringes at -20 °C for the same duration to induce cryogelation. After gelation, all samples were immersed in distilled water, which was periodically refreshed to remove unreacted species, and allowed to equilibrate until constant swelling was achieved. Finally, an additional set of cryogels was further prepared for vancomycin loading. Lyophilized Alt-C was cut into disc-shaped samples. 1 mg of vancomycin was dissolved in 1 mL of distilled water and vortexed. Then, 10 µL of this solution was applied to each disc and allowed to diffuse completely into the gel matrix. These vancomycin-loaded cryogels were designated as Alt-CV.

Characterizations

FTIR spectroscopy was performed to analyze the chemical structure of alternan, ECH, Alt-H, Alt-C and Alt-CV using a Bruker Tensor 27 FTIR spectrometer in the wavenumber range of 4000–400 cm^{-1}. The gels were weighed in three distinct states to evaluate their swelling behavior and determine the gel fraction: immediately after synthesis (m_0), at swelling equilibrium ($m_{swollen}$), and after subsequent drying (m_{dry}). The swelling equilibrium ratio (q_w) and gel fraction (W_g) were calculated according to Eqs. (1) and (2), where C represents the polymer concentration.

$$q_w = \frac{m_{swollen}}{m_{dry}} \tag{1}$$

$$W_g = \frac{m_{dry}}{m_0 * C} * 100 \tag{2}$$

Swelling kinetics were investigated by immersing dried gel samples in distilled water and recording their weights (m_t) at specific time intervals. The time-dependent gravimetric swelling ratio (m_{rel}) was calculated according to Eq. (3):

$$m_{rel} = \frac{m_t}{m_{dry}} \tag{3}$$

The morphology of the gels was examined using a ZEISS EVO 10 scanning electron microscope (SEM), and pore sizes were quantified using ImageJ software. Prior to analysis, the dry gel samples were coated with a thin gold/palladium layer to ensure electrical conductivity. Compression tests were performed using a Zwick/Roell Z0.5 TH testing machine, and the nominal stress (σ_{nom}), strain (ε), fracture strength (σ_f), fracture strain (ε_f), Young's modulus (E), and toughness (W) of the gel specimens in both dry and wet conditions were determined.

Antibacterial activity

Antibacterial activity was evaluated using the disc diffusion and time kill methods against four *S. aureus* strains with different antibiotic susceptibility profiles: oxacillin-susceptible *S. aureus* (OSSA), methicillin- and oxacillin-resistant *S. aureus* (MORSA), methicillin-resistant *S. aureus* (MRSA), and methicillin-susceptible *S. aureus* (MSSA). For both methods, overnight bacterial cultures were adjusted to a concentration of 10^8 CFU mL^{-1}, and the external surfaces of the gels were sterilized under UV irradiation prior to testing. In the disc diffusion assay, the prepared bacterial suspensions were evenly spread onto Mueller-Hinton agar plates. Disc-shaped Alt-C gel samples, vancomycin-loaded Alt-CV samples prepared by applying 10 µg of vancomycin onto each Alt-C gel disc, and commercial vancomycin discs containing an equivalent amount of vancomycin (10 µg per disc) were placed on the inoculated agar plates and incubated at 37 °C overnight. All experiments were performed in triplicate, and the results are reported as mean inhibition zone diameter ± standard deviation. For the time killing method, 10 µL of the bacterial suspension was applied dropwise onto each Alt-CV gel sample and vancomycin-loaded commercial blank disc, followed by incubation at room temperature for 30 min. The samples were then transferred into sterile bottles containing 10 mL of Mueller-Hinton broth. As a control, 10 µL of the bacterial suspension was directly inoculated into the broth without any test sample. All bottles were incubated at 37 °C with shaking at 180 rpm for 8 h. At the end of the incubation period, samples were collected and plated for viable colony enumeration [27]. Antimicrobial activity was quantified using the Eq. (4):

$$Log\ reduction\ in\ bacterial\ count = \log_{10}(A) - \log_{10}(B) \tag{4}$$

where A represents the bacterial count (CFU mL^{-1}) of the treated sample, and B that of the untreated control after incubation.

In vitro viability

Viability test was conducted using the direct contact method in accordance with ISO 10993-5, with modifications based on previously published studies, employing the L929 fibroblast cell line [28]. Briefly, the samples (Alt-C and Alt-CV) were sterilized under UV light for 1 h on each side. After sterilization, the samples were placed

in tubes containing complete growth medium and incubated at 37 °C for 24 h with continuous shaking at 120 rpm to generate the extracts. L929 cells were cultured in Dulbecco's Modified Eagle Medium supplemented with 10% fetal bovine serum and 1% penicillin-streptomycin. Cells were maintained under standard culture conditions (37 °C, 5% CO_2). Upon reaching 70–80% confluence in T-75 culture flasks, cells were detached using trypsin-EDTA and collected by centrifugation. The supernatant was discarded, and the cell pellet was resuspended in 1 mL of complete medium. Cell counting was performed using trypan blue exclusion with a Thoma hemocytometer to determine viable cell density. The required number of cells was subsequently diluted in growth medium for seeding. For the cytotoxicity assessment, cells were seeded into 96-well plates at a density of 5×10^3 cells per well and incubated for 24 h to allow attachment. The culture medium was then removed and replaced with the previously prepared 24 h extracts. Control wells received fresh complete medium. Cells were exposed to the extracts for 24 h and 48 h. Following the exposure period, 10 µL of MTT solution (5 mg/mL stock solution) was added to each well, and the plates were incubated in the dark for 4 h to allow for formazan formation. After incubation, 100 µL of dimethyl sulfoxide (DMSO) was added to each well to dissolve the formazan crystals, and the plates were kept in the dark for 20 min. The absorbance was measured at 570 nm by Biotek Epoch 2 Microplate Reader. The assays were conducted in triplicate as well. Cell viability (%) was calculated using the following Eq. (5):

$$Cell\ Viability\ (\%) = \frac{OD570_{Sample}}{OD570_{Control}} \times\ 100 \tag{5}$$

In Vitro wound scratch assay

The in vitro wound healing (scratch) assay was performed to evaluate cell migration capacity [27]. Briefly, 1×10^5 cells were seeded into 24-well plates and incubated for 24 h to allow the formation of a confluent monolayer. A linear scratch was then created in each well using a sterile 200 µL pipette tip to generate a defined wound area. Detached cells were carefully removed by washing the wells with 1× PBS. Subsequently, fresh complete medium was added to the control wells, while the prepared extracts were applied to the experimental groups. Wound closure was monitored by capturing two-dimensional images of the same wound regions at 0, 24, and 48 h using a light microscope.

Results and discussion

Upon extraction of alternan, ECH-mediated crosslinking was employed to couple alternan chains under alkaline conditions, resulting in the formation of a three-dimensional polymer network, as illustrated in Scheme 1 for cryogel synthesis. In the presence of NaOH, alternan hydroxyl groups are activated and promote epoxide ring opening of ECH, generating ether bridges between polysaccharide chains [29, 30].

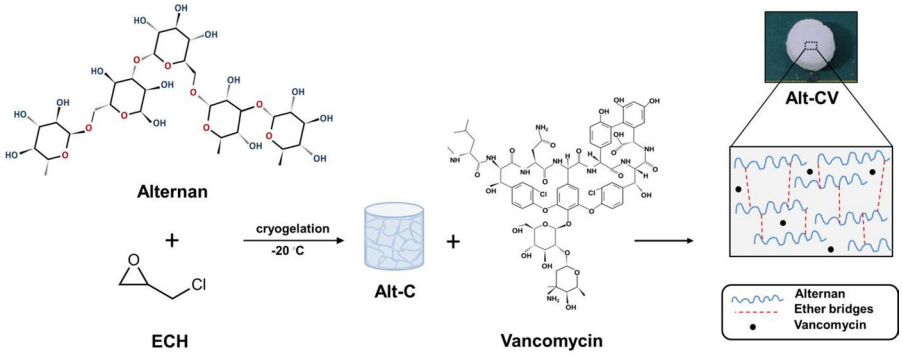

Scheme 1 Cryogel formation via ECH-mediated crosslinking of alternan under subzero conditions (cryogelation), illustrating representative ECH-derived ether bridges, followed by vancomycin loading into the resulting cryogel network

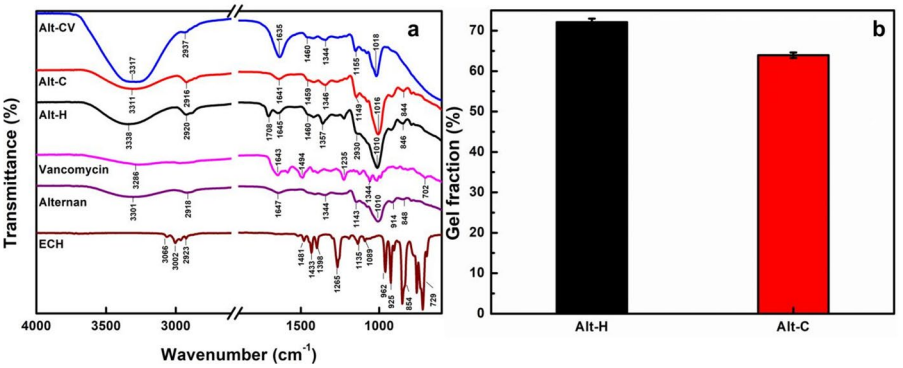

Fig. 1 **(a)** FTIR spectra of Alt-CV, Alt-C, Alt-H, vancomycin, alternan and ECH **(b)** Gel fraction percentages (W_g) of Alt-H and Alt-C

When these linkages occur between different chains, they produce the permanent cross-linked architecture responsible for gel formation.

The FTIR spectra of alternan, ECH, Alt-H, Alt-C, and Alt-CV are shown in Fig. 1a. The spectrum of alternan exhibits a broad absorption band around 3300 cm^{-1}, attributed to O-H stretching vibrations typical of polysaccharides, along with a band near 2900 cm^{-1} corresponding to C-H stretching. The absorption band observed at approximately 1650 cm^{-1} is associated with absorbed water, which is commonly detected in carbohydrate-based materials. In addition, the strong band centered around 1020 cm^{-1} is assigned to C-O-C and C-O stretching vibrations of glycosidic linkages, supporting the polysaccharide backbone of alternan. These findings align well with previous reports on polysaccharide-based hydrogel studies. For instance, Hu et al. reported that konjac glucomannan hydrogels exhibit a broad O-H stretching band in the 3600 –3300 cm^{-1} range, C-H stretching around 2925 cm^{-1}, and a strong band near 1024 cm^{-1} arising from glycosidic C-O and C-O-C vibrations, which were taken as evidence that the polysaccharide backbone remains intact after gel formation

[31]. The band around 1650 cm^{-1} assigned to bound water is also consistent with other polysaccharide systems, where bands in the 1635–1640 cm^{-1} region increase in intensity due to solvent-associated water [32]. These findings are also comparable with reported EPS-based hydrogels. In a β-(1→6)-D-glucan exopolysaccharide hydrogel, the region between 3600 and 2997 cm^{-1} was described as characteristic of polysaccharide O-H stretching vibrations, while a band around 1600 cm^{-1} was attributed to stretching vibration of the glucose ring structure [33]. Similarly, *Nostoc sp.* EPS hydrogels exhibit a broad absorption band centered at approximately 3320 cm^{-1}, assigned to O-H stretching common to EPS systems, highlighting the conserved spectral features of microbial exopolysaccharide networks [34]. Following crosslinking with ECH, the FTIR spectra of both Alt-H and Alt-C exhibit a broadening of the band in the 1000–1150 cm^{-1} region, consistent with the formation of newly developed C-O-C ether linkages resulting from the reaction between the epoxide groups of ECH and the hydroxyl groups of alternan, indicating the formation of a cross-linked polymer network. Importantly, the preservation of the characteristic alternan bands in these spectra suggests that the polysaccharide backbone remains intact after gelation under both conventional and cryogenic conditions. This interpretation is consistent with other studies on cross-linked polysaccharide networks, where modifications in the 1000–1150 cm^{-1} region are attributed to network formation rather than backbone degradation [35, 36]. The Alt-CV exhibits additional absorption features overlapping with those of the polymer matrix, particularly in the regions associated with O-H and N-H stretching vibrations, suggesting the successful incorporation of vancomycin into the cryogel structure. The overall similarity between the spectra of loaded and unloaded cryogels indicates that drug loading does not significantly alter the chemical structure of the alternan-based network and is incorporated through non-covalent interactions such as hydrogen bonding [37]. The gel fraction and swelling behavior of the Alt-H, Alt-C, and Alt-CV gels were systematically investigated to reveal the relationship between the network structure and water uptake properties. The gel fraction values, presented in Fig. 1b, show that Alt-H possesses a higher degree of crosslinking with 72.09 ± 0.91% compared to Alt-C with 63.94 ± 0.66%.

The swelling equilibrium ratios (q_w), shown in Fig. 2a, reveal that Alt-C exhibits a significantly higher swelling capacity with 14.01 ± 0.19 than Alt-H with 10.03 ± 0.09. This pronounced swelling behavior of Alt-C is attributable to its macroporous network structure, which facilitates more extensive water uptake [9, 38]. Such structure-property relationships have been observed in other polysaccharide systems and are linked to enhanced water uptake behavior. For example, Pacelli et al. reported dextran methacrylate-PEG dimethacrylate cryogels exhibited enhanced swelling and pronounced porosity compared to their corresponding hydrogels due to the macroporous cryogel network, demonstrating that cryogelation increases water uptake due to the formation of a macroporous network [39]. Alves et al. revealed that cross-linked dextran hydrogels exhibit swelling ratios around 11, a value comparable to Alt-H and indicative of the restrictive nature of denser hydrogel networks. In contrast, the higher swelling capacity observed in Alt-C and Alt-CV emphasizes that cryogelation promotes a more open architecture capable of absorbing water far more efficiently than conventionally formed hydrogels [40]. Notably, Alt-CV displays the highest swelling equilibrium ratio 15.68 ± 0.16, indicating that vancomycin incorporation

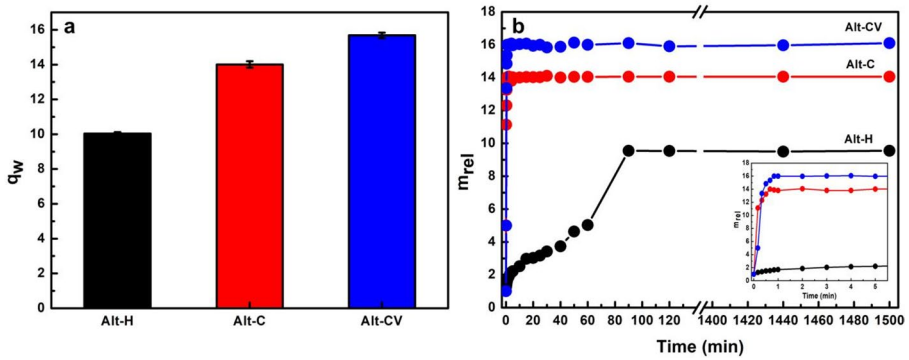

Fig. 2 **(a)** Swelling equilibrium ratios (q_w) of Alt-H, Alt-C and Alt-CV **(b)** Swelling kinetics of gels depending on time (minutes)

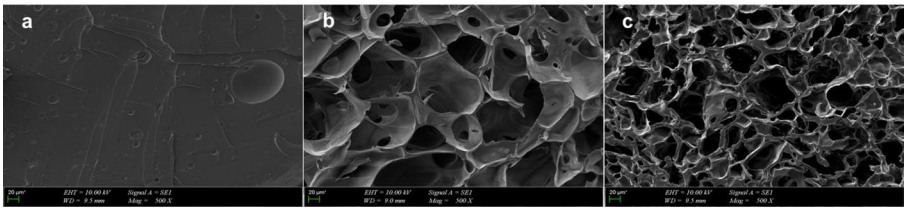

Fig. 3 SEM images of alternan-based gels at 500× magnification: **(a)** Alt-H, **(b)** Alt-C, and **(c)** Alt-CV, illustrating differences in network morphology across hydrogel, cryogel, and vancomycin-loaded cryogel structures

does not hinder water uptake and may slightly enhance swelling through additional hydrophilic interactions within the cryogel matrix.

The swelling kinetics profiles, illustrated in Fig. 2b, further support these observations. Both Alt-C and Alt-CV exhibit a rapid and steep initial increase in the time-dependent gravimetric swelling ratio (m_{rel}), reaching swelling equilibrium within approximately 1 min, as more clearly illustrated in the inset of Fig. 2b. While Alt-C reaches a maximum m_{rel} value of approximately 14, Alt-CV shows slightly higher maximum m_{rel} values in the range of 15–16, confirming that vancomycin loading preserves the fast swelling kinetics and slightly increases the swelling capacity. In contrast, Alt-H displays a slower and more gradual swelling behavior, reaching equilibrium only after prolonged immersion and exhibiting lower maximum m_{rel} values of 9–10. Together, these results demonstrate that cryogels possess a more open network structure than hydrogels, leading to enhanced and faster water absorption, while vancomycin loading maintains these advantageous swelling characteristics.

The SEM analyses provide clear insight into how the gelation method and vancomycin incorporation influence the internal structure of the alternan-based gels. As shown in Fig. 3a, Alt-H displays a dense and compact morphology with no evident interconnected pores. In contrast, both Alt-C and Alt-CV illustrate an open and continuous macroporous structure (Fig. 3b and c). This marked difference arises from the cryogenic gelation process, in which ice crystals temporarily occupy the polymer

solution and define the pore network during crosslinking. After thawing, the removal of these ice crystals leaves behind large, interconnected pores that are not formed during conventional gelation.

Figure 4 further reveals the internal morphology of the cryogels, showing thin pore walls and a highly interconnected network that favors rapid fluid penetration and transport. Quantitative pore size analysis supports these observations, with Alt-C exhibiting a broad pore size distribution and an average pore size of 84 ± 31 µm (Fig. 4b). Such pore dimensions are advantageous for wound dressing applications, as they facilitate rapid swelling and effective exudate management. Previous studies have also indicated that pore sizes in the range of 20–120 µm are favorable for wound healing, thus the pore sizes measured for cryogel samples fall within the ranges reported for other exopolysaccharide cryogels [41–43], supporting their suitability as wound dressings. After vancomycin loading, Alt-CV maintains its macroporous and interconnected structure (Fig. 4c), while the average pore size decreases to 64 ± 27 µm (Fig. 4d). This reduction is due to partial coverage of the pore surfaces by vancomycin rather than pore collapse or significant structural densification. Importantly, the interconnected nature of the pore network is preserved, indicating that drug incorporation does not hinder mass transport through the cryogel. From a wound dressing perspective, the presence of an open, interconnected macroporous network is advantageous, as it facilitates rapid fluid absorption, effective transport of therapeutic agents, and close conformity to the wound surface. Consequently, the SEM

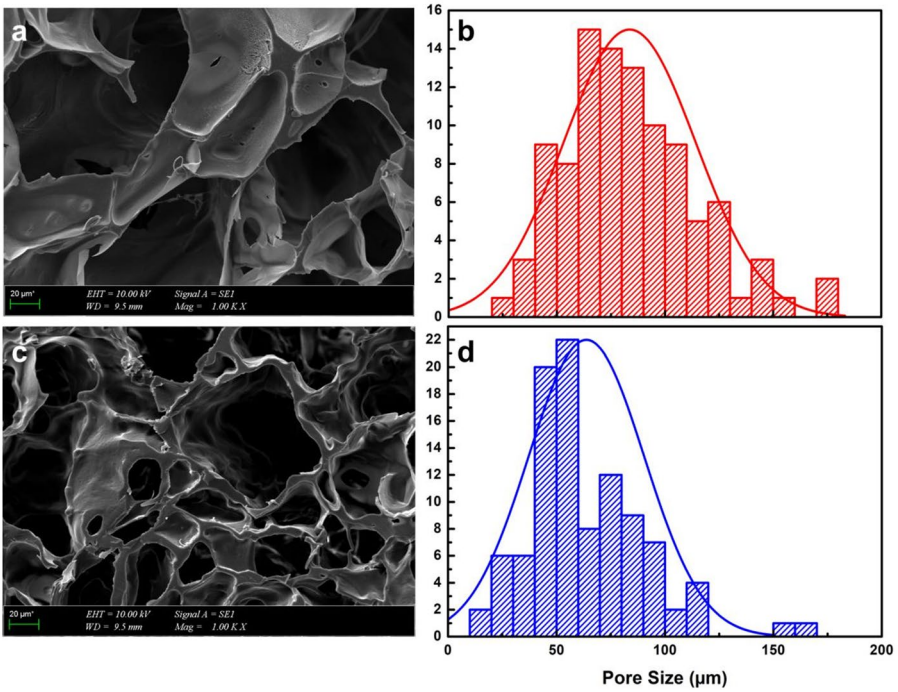

Fig. 4 **(a)** SEM image of Alt-C at 1000x magnification **(b)** Pore size distribution histogram of Alt-C **(c)** SEM image of Alt-CV at 1000x magnification **(d)** Pore size distribution histogram of Alt-CV

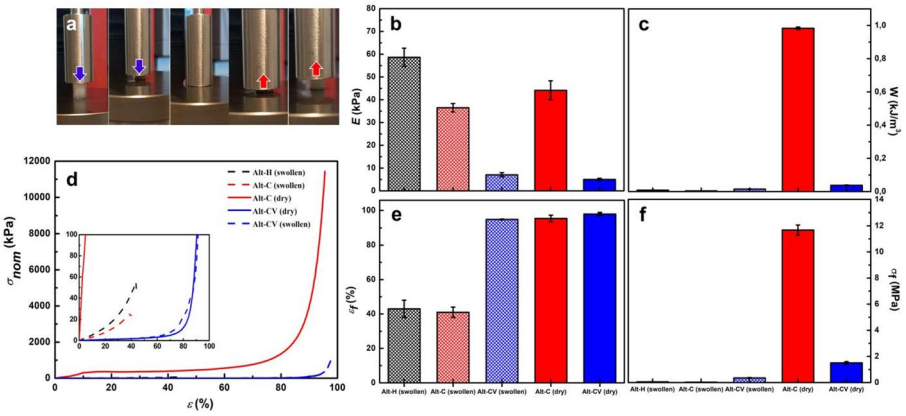

Fig. 5 **(a)** Compression test of swollen Alt-C **(b)** Young's modulus *E* of swollen Alt-H, swollen Alt-C, swollen Alt-CV, dry Alt-C and dry Alt-CV **(c)** Toughness *W* of these gels **(d)** Stress-strain curves of the gels **(e)** Fracture strain ε_f of the gels **(f)** Fracture strength σ_f of the gels

Table 1 Compressive mechanical parameters of the gel samples

State	Parameters	Alt-H	Alt-C	Alt-CV
Dry	*E* (kPa)	-	44.15 ± 4.14	5.04 ± 0.45
	σ_f (kPa)		11,675 ± 385	1505 ± 98
	ε_f (%)		95.5 ± 1.9	98 ± 0.85
	W (kPa)		983.5195 ± 7.55	37.4569 ± 2.19
Swollen	*E* (kPa)	58.62 ± 4.03	36.48 ± 1.87	7.06 ± 0.90
	σ_f (kPa)	53.85 ± 4.75	26.1 ± 1.35	353.86 ± 29.03
	ε_f (%)	43 ± 5	41 ± 3	94.95 ± 0.24
	W (kPa)	8.235 ± 0.58	3.8626 ± 0.22	14.898 ± 1.183

observations demonstrate that alternan-based cryogels offer a robust macroporous platform in which antibacterial functionality can be introduced without compromising the structural characteristics required for wound management.

The compressive mechanical properties of Alt-H, Alt-C, and Alt-CV were evaluated by uniaxial compression tests, as illustrated in Fig. 5. For this purpose, cylindrical samples with a diameter and a height of 5 mm were measured both in dry and swollen states. The corresponding mechanical parameters, including Young's modulus (*E*), toughness (*W*), fracture strain (ε_f), and fracture strength (σ_f), are summarized in Table 1. Figure 5a shows that upon application and subsequent removal of a compressive load, the samples readily recover their original shape without any visible cracking or structural damage. *E* values obtained from compression tests are presented in Fig. 5b. In the swollen state, Alt-H exhibited a higher stiffness of 58.62 ± 4.03 kPa compared to Alt-C with 36.48 ± 1.87 kPa, which can be attributed to its higher gel fraction and denser network structure. In the dry state, cryogels showed notably higher modulus 44.15 ± 4.14 kPa, whereas Alt-CV exhibited a substantially lower modulus 5.04 ± 0.45 kPa, indicating increased network compliance after drug loading. This softening contrasts with the higher stiffness reported for exopolysaccharide dextran and bacterial cellulose-based macroporous hydrogel scaffolds developed for cartilage appli-

cations, underlining that the alternan gels are mechanically tuned for softer tissue environments [44]. Nevertheless, the alternan cryogels combine exceptionally high deformability with markedly higher compressive strength, highlighting their ability to sustain large deformations while bearing substantial loads.

W values of the gels are shown in Fig. 5c. In the swollen state, Alt-H exhibited higher toughness than Alt-C, reflecting their greater energy absorption capacity under compression. In contrast, dry Alt-C demonstrated exceptionally high toughness with 983.52 ± 7.55 kJ/m³, while Alt-CV showed lower but still appreciable toughness 37.46 ± 2.19 kJ/m³, consistent with their softer and more compliant mechanical response after drug incorporation. In a related study, EPS-based hydrogels derived from *Alteromonas macleodii* Mo169 cross-linked with Fe^{3+} reported that the toughness varied broadly from 0.5 to 42.5 kJ/m³ depending on the polymer/cross-linker ratio, accompanied by Young's modulus values ranging from 47 to 329.3 kPa and rupture strains of 49–86% [45]. Relative to that range, the alternan gels exhibit competitive stiffness in the swollen state while achieving notably higher failure strains in the dry state, indicating superior compressive deformability without catastrophic collapse. This combination of high deformability and recoverable toughness is in line with other exopolysaccharide-based cryogels, such as platelet-lysate/oxidized-dextran systems, which have been described as elastic, compressible scaffolds capable of withstanding large cyclic deformations without structural collapse [43].

Nominal stress-strain (σ_{nom}-ε) curves of the gels are presented in Fig. 5d. In the swollen state, both Alt-H and Alt-C displayed typical soft and elastic behavior. In contrast, dry Alt-C exhibited a steep stress-strain response indicative of high stiffness and strength, whereas Alt-CV showed a more compliant stress-strain profile while maintaining large deformation before failure. ε_f values summarized in Fig. 5e indicate that swollen Alt-H and Alt-C exhibit comparable deformation at failure ~ 41–43%. In the dry state, both Alt-C and Alt-CV maintained very high fracture strains ~ 95.5% and ~ 98%, respectively, demonstrating excellent deformability even under high compressive loads. σ_f values shown in Fig. 5f further highlight the influence of gel state and drug loading. In the swollen state, Alt-H withstood higher stresses 53.85 ± 4.75 kPa than Alt-C with 26.1 ± 1.35 kPa. In the dry state, Alt-C exhibited a very high fracture strength 11,675 ± 385 kPa, whereas Alt-CV showed reduced strength with 1505 ± 98 kPa, indicating that vancomycin incorporation reduces stiffness and strength while preserving high deformability. A similar mechanical behavior has been reported for vancomycin-loaded gelatin/poly ((N-isopropyl acrylamide)-co-N-(methylol acrylamide)) hydrogel wound dressing, where drug incorporation decreased compressive strength while maintaining high failure strain, indicating that antibiotic loading primarily softens the network without impairing its ability to sustain large compressive deformations [25].

These results demonstrate that both gel state and network structure strongly influence the mechanical response of the gels. While Alt-H exhibit superior mechanical stability in the swollen state, Alt-C particularly in the dry state shows remarkable strength and deformability. Interestingly, for vancomycin-loaded gel samples, the elastic modulus, *E* values did not change significantly in both dry and wet conditions. Furthermore, while the percentage elongation at break, ε_f of Alt-C decreased from 95.5% to 41% when changing from dry to wet, Alt-CV only changed by 3%. When

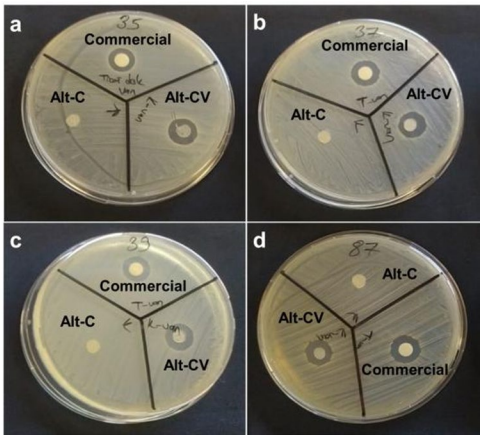

Fig. 6 Antibacterial activity of Alt-C, Alt-CV, and the vancomycin-loaded commercial disc against different *S. aureus* strains: **(a)** OSSA, **(b)** MORSA, **(c)** MRSA, and **(d)** MSSA

Table 2 Mean inhibition zone diameters (mm) of vancomycin-containing cryogels and vancomycin-loaded commercial discs against different microorganisms ($n = 3$)

Microorganism	Alt-C	Alt-CV	Commercial Disc
OSSA	0	13 ± 0.5	11.5 ± 0.5
MORSA	0	13 ± 0.5	12 ± 0.5
MRSA	0	13.5 ± 0.5	12 ± 0.5
MSSA	0	11.5 ± 0.5	12 ± 0.5

the fracture strength, σ_f values were examined, the values decreased from 11,675 to 1505 kPa in the dry condition when vancomycin was loaded, while they increased from 26 to 354 kPa in the wet condition. The toughness, W values of the gel samples also exhibit a similar trend. Therefore, it is clearly seen that vancomycin loading on the samples resulted in a significant improvement in the properties of the swollen state. Notably, vancomycin loading modulates the mechanical properties of cryogels by reducing stiffness and strength while maintaining high strain tolerance, which may be advantageous for applications requiring flexible yet resilient materials.

Antibacterial activity results

The antibacterial activity of the Alt-CV was investigated against four *S. aureus* strains with different antibiotic resistance profiles, namely OSSA, MORSA, MRSA, and MSSA, using the disc diffusion method as illustrated in Fig. 6. Alt-C was used as negative control to assess any intrinsic antibacterial effect of the polymer matrix, while commercial discs containing the same amount of vancomycin were used as positive controls for comparison.

The control Alt-C did not produce any inhibition zones against the tested microorganisms, confirming that the alternan-based cryogel matrix itself does not exhibit antibacterial activity. Conversely, clear inhibition zones were observed for both Alt-CV and the commercial vancomycin discs against all tested strains, demonstrating effective antibacterial action. The inhibition zone diameters are summarized in Table 2 where Alt-CV exhibited inhibition zones ranging from 11.5 ± 0.5 to 13.5 ± 0.5 mm,

which were comparable to those obtained with the commercial vancomycin discs, as 11.5 ± 0.5 to 12 ± 0.5 mm. The comparable inhibition zone diameters indicate that vancomycin retains its antibacterial efficacy after incorporation into the cryogel matrix and is released in sufficient amounts to inhibit bacterial growth. Importantly, the antibacterial activity was observed against both methicillin-resistant and methicillin-sensitive *S. aureus* strains, highlighting the effectiveness of Alt-CV across different resistance profiles. These results are consistent with the antibacterial activity reported for other vancomycin-loaded polysaccharide-based wound dressings. Oxidized hyaluronic acid hydrogels loaded with vancomycin showed inhibition zones of 9–21 mm against MRSA, depending on the antibiotic loading level, demonstrating that vancomycin retains its activity when embedded in a hydrated polymer network [46]. Similarly, maltodextrin-chitosan copolymer hydrogels designed for local vancomycin delivery exhibited antibacterial inhibition against *S. aureus*, and also showed zone diameters reaching 31 ± 1 mm against *E. coli*, confirming that biopolymer-bound vancomycin can effectively diffuse and suppress pathogenic growth in wound applications [47]. These comparisons confirm that Alt-CV provides antimicrobial performance within the effective range of established vancomycin-releasing wound dressings, and enables sufficient drug release to inhibit both methicillin-resistant and methicillin-sensitive *S. aureus* strains while additionally offering the structural advantages of a macroporous cryogel platform. To confirm the results obtained from the disc diffusion assay, antibacterial activity was further assessed using the time kill method. Viable bacterial colonies recovered from agar plates were enumerated (Fig. 7), and the logarithmic reduction was calculated by comparing bacterial counts in the treated samples with those of the untreated control after 8 h of incubation. Both the Alt-CV gel and the vancomycin-loaded blank disc reduced all tested *S. aureus* strains by approximately 1–2 log units. No noticeable variation in bacterial reduction was

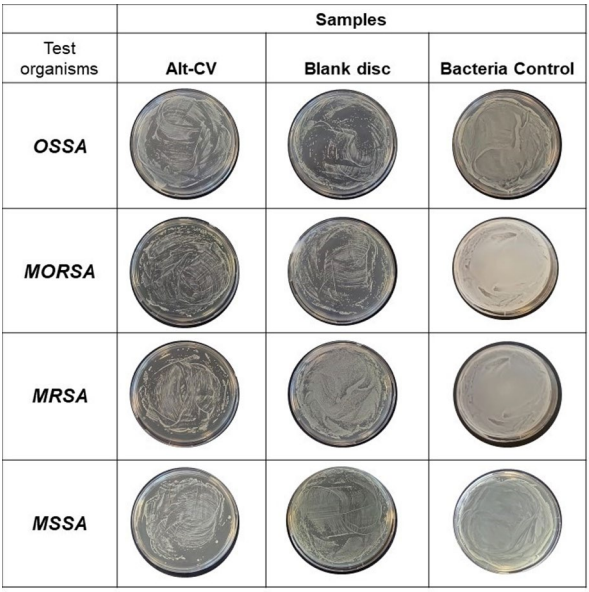

Fig. 7 Representative agar plates showing viable bacterial colonies recovered from undiluted samples

observed between the Alt-CV gel and the vancomycin-loaded blank disc across the different *S. aureus* strains. These findings are in agreement with the disc diffusion results, further supporting the similar antibacterial performance of the two samples. Overall, the observed antibacterial efficacy highlights the potential of Alt-CV as a vancomycin-releasing wound dressing capable of controlling *S. aureus* infections irrespective of methicillin susceptibility.

In vitro viability results

Evaluation of the effects of the produced materials on healthy mammalian cells is critically important in terms of biocompatibility and safety for potential therapeutic applications. Therefore, the effects of the samples on L929 cells were investigated using the MTT assay. Alt-CV and Alt-C were applied to the cells at different concentrations. Untreated L929 cells were used as the negative control group. Figure 8a and b present the cell viability of samples treated for 24 and 48 h, respectively.

At 24 h (Fig. 8a), cell viability in the negative control group ranged between approximately 95–100% across all concentrations. In the Alt-CV group, cell viability varied between approximately 72–85% in a concentration-dependent manner. At the highest concentration (50 µg/mL), viability was approximately 72%, whereas a gradual increase in cell viability was observed with decreasing concentration, exceeding 80% at lower concentrations (0.78–0.39 µg/mL). In the Alt-C group, cell viability ranged between approximately 60–70%. Notably, in the 6.25–12.5 µg/mL concentration range, viability decreased to approximately 60–65%, showing lower values compared to the Alt-CV group. At 24 h, Alt-CV exhibited higher cell viability than Alt-C at all tested concentrations.

At 48 h (Fig. 8b), cell viability in the negative control group again remained within the 95–100% range. In the Alt-CV group, cell viability ranged between approximately 65–85%. At the highest concentration (50 µg/mL), viability was approximately 65%, while at moderate and low concentrations, viability reached 80–85%. In the Alt-C group, cell viability ranged between approximately 73–82%. Compared to the 24 h

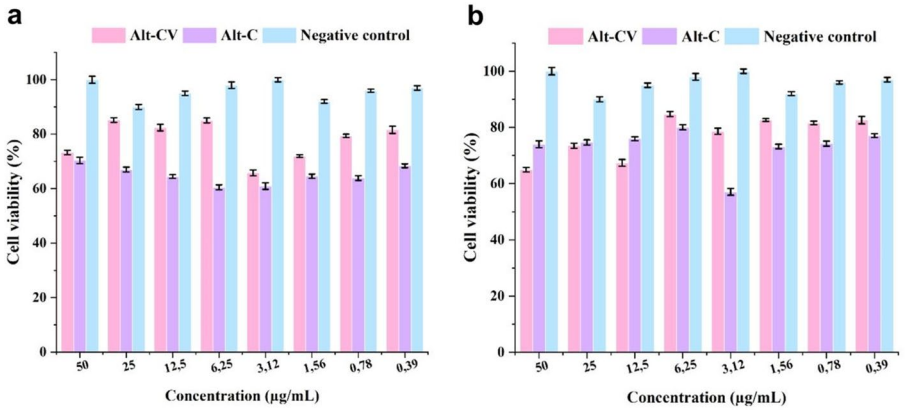

Fig. 8 **(a)** Cell viability of L929 cells treated with different concentrations of Alt-CV, Alt-C and negative control for 24, **(b)** 48 h (The error bars represent the standard deviation from the mean ($n = 3$)

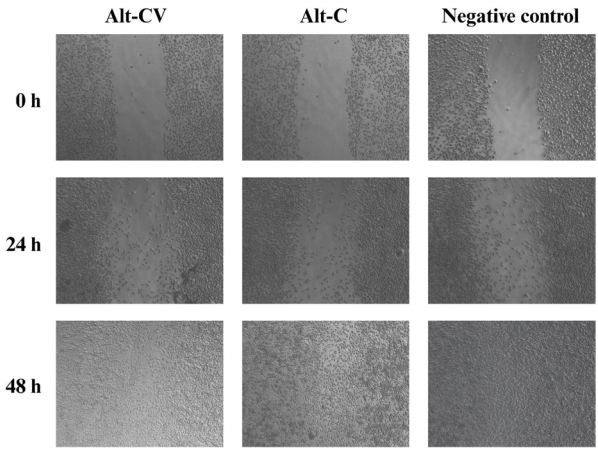

Fig. 9 Microscopic images of the wound scratch assay for the samples at 0, 24, and 48 h

results, a noticeable increase in viability was observed, particularly at moderate and low concentrations, where viability exceeded 75%. At 48 h, the difference between the two materials decreased. At the highest concentration, Alt-CV exhibited lower viability, whereas at some moderate and low concentrations, Alt-C showed comparable or slightly higher values.

Overall, cell viability remained above 60% for both materials, with values exceeding 70% particularly at low and moderate concentrations. According to ISO 10993-5 standards, cell viability above 70% is generally considered indicative of non-cytotoxic behavior. In this context, both materials can be regarded as biocompatible at low and moderate concentrations. The obtained findings demonstrate that at 24 h, Alt-CV provided higher cell viability compared to Alt-C. This suggests that vancomycin incorporation did not adversely affect the cellular compatibility of the cryogel matrix and may even confer a relative advantage in terms of biocompatibility.

In vitro wound scratch assay

Microscopic images of the wound scratch assay are presented in Fig. 9. The wound healing assay demonstrated time-dependent differences in fibroblast migration among the experimental groups. At 0 h, comparable scratch widths confirmed similar initial conditions. After 24 h, the negative control exhibited substantial migration into the wound area, indicating active cell movement and early closure. A similar migratory pattern was observed in the Alt-CV group, where cells progressed into the scratched region in a relatively organized manner and the wound gap was markedly reduced. In contrast, the Alt-C group showed comparatively slower migration, with a visibly wider remaining gap at the same point. By 48 h, near-complete closure was observed in the negative control, while Alt-CV displayed pronounced wound narrowing and increased cellular density within the previously cell-free region. Although Alt-C also demonstrated progressive closure over time, the migratory response appeared less extensive, and less uniform compared to Alt-CV. These findings indicate that vancomycin incorporation did not impair fibroblast migratory capacity and may have contributed to a more favorable cellular response in terms of wound closure dynamics.

Moreover, the enhanced migration observed in the Alt-CV group is consistent with the cytocompatibility profile obtained from the MTT assay.

Conclusion

This work establishes alternan as a viable and previously unexplored exopolysaccharide for the fabrication of functional hydrogel and cryogel biomaterials. Structural analyses confirmed that alternan preserves its characteristic α-(1→3)/α-(1→6) glycosidic architecture following ECH-mediated crosslinking and subsequent drug loading, ensuring the integrity of the polysaccharide matrix throughout material processing. Clear structure-property relationships emerged between the two gelation pathways. Cryogelation produced cryogels with an interconnected macroporous architecture, leading to higher swelling capacity and more rapid fluid uptake than hydrogels prepared at room temperature. SEM observations verified that the porous architecture of the cryogels remained intact after vancomycin incorporation. Mechanically, the cryogels displayed high deformability and shape recovery, resulting in a softer and more compliant structure suitable for conformal contact with complex wound geometries-a critical criterion for patient comfort and atraumatic application. The antibacterial studies demonstrated that vancomycin-loaded cryogels effectively inhibited both methicillin-sensitive and methicillin-resistant *S. aureus*, confirming that the porous alternan network supports efficient antibiotic incorporation and release without loss of antimicrobial potency. Overall, the synergy of macroporosity, rapid fluid absorption, mechanical compliance, and robust antibacterial activity positions alternan-based cryogels as a compelling platform for advanced wound dressing applications. By introducing alternan into the gel-design landscape, this study broadens the range of functional exopolysaccharide biomaterials and highlights the promise of alternan-based cryogels as multifunctional dressings capable of managing wound exudate while providing localized antibacterial protection. Future studies will address the quantitative evaluation of drug-loading efficiency, release kinetics, and vancomycin distribution within the cryogel matrix to further define the drug delivery performance and translational potential of alternan-based cryogels for advanced wound dressing applications.

Acknowledgements Not applicable.

Author contributions Sanem Bulut: Methodology, Investigation, Data curation, Writing-original draft. Semra Taşdurmazlı: Investigation. Esra Bedir: Investigation. Esra Su: Investigation, Writing-original draft. Kader Korkmaz Edis: Investigation. Enes Dertli: Investigation, Writing-original draft. Tülin Özbek: Investigation, Writing-original draft. Mehmet Murat Ozmen: Supervision, Resources, Project administration, Writing-original draft. All authors reviewed the manuscript.

Funding Open access funding provided by the Scientific and Technological Research Council of Türkiye (TÜBİTAK).

Data availability All data is available upon reasonable request.

Declarations

Conflict of interest The authors declare that they have no conflict of interest.

Open Access This article is licensed under a Creative Commons Attribution 4.0 International License, which permits use, sharing, adaptation, distribution and reproduction in any medium or format, as long as you give appropriate credit to the original author(s) and the source, provide a link to the Creative Commons licence, and indicate if changes were made. The images or other third party material in this article are included in the article's Creative Commons licence, unless indicated otherwise in a credit line to the material. If material is not included in the article's Creative Commons licence and your intended use is not permitted by statutory regulation or exceeds the permitted use, you will need to obtain permission directly from the copyright holder. To view a copy of this licence, visit http://creativecommons.org/licenses/by/4.0/.

References

1. Hodge JG, Zamierowski DS, Robinson JL, Mellott AJ (2022) Evaluating polymeric biomaterials to improve next generation wound dressing design. Biomater Res 26:1. https://doi.org/10.1186/s40824-022-00291-5
2. Kadri HJ, Ahmed F, Rahman MH, Mondal MIH (2025) Synthesis and characterisation of starch-g-polyacrylamide-co-polylactic acid hydrogel for the potential wound dressing application. Polym Bull 82:7917–7941. https://doi.org/10.1007/s00289-025-05840-1
3. Akin B, Ozmen MM (2022) Antimicrobial cryogel dressings towards effective wound healing. Prog Biomater 11:331–346. https://doi.org/10.1007/s40204-022-00202-w
4. Górska A, Baran E, Knapik-Kowalczuk J, Szafraniec-Szczęsny J, Paluch M, Kulinowski P, Mendyk A (2024) Physically cross-linked PVA hydrogels as potential wound dressings: How freezing conditions and formulation composition define cryogel structure and performance. Pharmaceutics 16:1388. https://doi.org/10.3390/pharmaceutics16111388
5. Olcer Z, Ozmen MM, Sahin ZM, Yilmaz F, Tanriseven A (2013) Highly efficient method towards in situ immobilization of invertase using cryogelation. Appl Biochem Biotechnol 171:2142–2152. https://doi.org/10.1007/s12010-013-0507-5
6. Savina IN, Zoughaib M, Yergeshov AA (2021) Design and assessment of biodegradable macroporous cryogels as advanced tissue engineering and drug carrying materials. Gels 7:79. https://doi.org/10.3390/gels7030079
7. Otulakowski Ł, Klama-Baryła A, Celny A, Kasprów M, Hercog A, Godzierz M, Sitkowska A, Kadłubowski S, Jaworska M, Chmielik E, Trzebicka B, Utrata-Wesołek A (2023) Laminar biomaterial composite of PVA cryogel with amnion as potential wound dressing. Polymers 15:2955. https://doi.org/10.3390/polym15132955
8. Xu G, Xu N, Ren T, Chen CH, Ding L, Chen Y, Li G, Yu Y (2022) Multifunctional chitosan/silver/tannic acid cryogels for hemostasis and wound healing. Int J Biol Macromol 208:760–771. https://doi.org/10.1016/j.ijbiomac.2022.03.174
9. Sen T, Ozcelik B, Ozmen MM (2019) Tough and hierarchical porous cryogel scaffolds preparation using n-butanol as a non-solvent. Int J Polym Mater Polym Biomater 68:411–416. https://doi.org/10.1080/00914037.2018.1452225
10. Li Y, Yang Z, Sun Q, Xu R, Li R, Wu D, Huang R, Wang F, Li Y (2023) Biocompatible cryogel with good breathability, exudate management, antibacterial and immunomodulatory properties for infected diabetic wound healing. Adv Sci 10. https://doi.org/10.1002/advs.202304243
11. Ozmen MM, Okay O (2004) Non-Gaussian elasticity of poly(2-acrylamido-2-methylpropane sulfonic acid) gels. Polym Bull 52:83–90. https://doi.org/10.1007/s00289-004-0247-3
12. Su E, Okay O (2019) Cryogenic formation-structure-property relationships of poly(2-acrylamido-2-methyl-1-propanesulfonic acid) cryogels. Polymer 178:121603. https://doi.org/10.1016/j.polymer.2019.121603
13. Hamidi M, Jafari H, Siminska-Stanny J, Okoro OV, Fatimi A, Shavandi A (2022) Anionic exopolysaccharide from *Cryptococcus laurentii* 70766 as an alternative for alginate for biomedical hydrogels. Int J Biol Macromol 212:370–380. https://doi.org/10.1016/j.ijbiomac.2022.05.133

14. Mohd Nadzir M, Nurhayati RW, Idris FN, Nguyen MH (2021) Biomedical applications of bacterial exopolysaccharides: A review. Polymers 13:530. https://doi.org/10.3390/polym13040530
15. Nguyen H-T, Pham T-T, Nguyen P-T, Le-Buanec H, Rabetafika HN, Razafindralambo HL (2024) Advances in microbial exopolysaccharides: Present and future applications. Biomolecules 14:1162. https://doi.org/10.3390/biom14091162
16. Ng JY, Obuobi S, Chua ML, Zhang C, Hong S, Kumar Y, Gokhale R, Ee PLR (2020) Biomimicry of microbial polysaccharide hydrogels for tissue engineering and regenerative medicine - A review. Carbohydr Polym 241:116345. https://doi.org/10.1016/j.carbpol.2020.116345
17. Chen Z, Ni D, Zhang W, Stressler T, Mu W (2021) Lactic acid bacteria-derived α-glucans: From enzymatic synthesis to miscellaneous applications. Biotechnol Adv 47:107708. https://doi.org/10.1016/j.biotechadv.2021.107708
18. İspirli H, Yüzer MO, Skory C, Colquhoun IJ, Sağdıç O, Dertli E (2019) Characterization of a glucansucrase from *Lactobacillus reuteri* E81 and production of malto-oligosaccharides. Biocatal Biotransform 37:421–430. https://doi.org/10.1080/10242422.2019.1593969
19. İspirli H, Korkmaz K, Arioglu-Tuncil S, Bozkurt F, Sağdıç O, Tunçil YE, Narbad A, Dertli E (2023) Utilisation of an active branching sucrase from *Lactobacillus kunkeei* AP-37 to produce techno-functional poly-oligosaccharides. Int J Biol Macromol 236:123967. https://doi.org/10.1016/j.ijbiomac.2023.123967
20. Yang Q, Peng J, Xiao H, Xu X, Qian Z (2022) Polysaccharide hydrogels: Functionalization, construction and served as scaffold for tissue engineering. Carbohydr Polym 278:118952. https://doi.org/10.1016/j.carbpol.2021.118952
21. Cifuente JO, Colleoni C, Kalscheuer R, Guerin ME (2024) Architecture, function, regulation, and evolution of α-glucans metabolic enzymes in prokaryotes. Chem Rev 124:4863–4934. https://doi.org/10.1021/acs.chemrev.3c00811
22. Liu Y, Qin J, Khan IM, Xiao H, Miao M, Chen G (2025) Alternan as a glucan with miscellaneous applications: Properties, preparation, and health efficacies. Food Chem 490:145140. https://doi.org/10.1016/j.foodchem.2025.145140
23. Tiwari S, Kavitake D, Devi PB, Halady Shetty P (2021) Bacterial exopolysaccharides for improvement of technological, functional and rheological properties of yoghurt. Int J Biol Macromol 183:1585–1595. https://doi.org/10.1016/j.ijbiomac.2021.05.140
24. Daaboul M, Akkaya A, Kanlı Z, Gündüz O, Aydın B, Alarcin E, Ozmen MM, Topuzogullari M (2025) Nanoparticle-embedded GelMA/NIPAm hydrogels: A temperature-responsive hybrid system for controlled drug release. https://doi.org/10.1002/mabi.202400635. Macromol Biosci:e00635
25. Tang Y, Shu X, He G, Zhang Y, Zhao Y, Yuan H, Yu J, Guo J, Chen Q (2024) Vancomycin-loaded hydrogels with thermal-responsive, self-peeling, and sustainable antibacterial properties for wound dressing. J Mater Chem B 12:752–761. https://doi.org/10.1039/D3TB02084C
26. Dertli E, Colquhoun IJ, Côté GL, Le Gall G, Narbad A (2018) Structural analysis of the α-D-glucan produced by the sourdough isolate *Lactobacillus brevis* E25. Food Chem 242:45–52. https://doi.org/10.1016/j.foodchem.2017.09.017
27. Akin B, Akgul B, Tasdurmazli S, Abamor ES, Ozbek T, Ozcelik B, Su E, Ozmen MM (2024) Tannic acid incorporated antibacterial polyethylene glycol based hydrogel sponges for management of wound infections. Macromol Biosci 24:202400101. https://doi.org/10.1002/mabi.202400101
28. Gokkaya Ozburun D, Hancer H, Findikli B, Ozbek T, Ozmen MM, Topuzogullari M (2025) Quaternized Poly(4-vinylpyridine-co-N-2-hydroxypropylmethacrylamide) and antibacterial peptide linear conjugates: Synthesis, characterization, and bioactivity. Eur Polym J 222:113615. https://doi.org/10.1016/j.eurpolymj.2024.113615
29. El-Naggar SA, El-Barbary AA, Hafez YA, Salama WM, Elkholy HM, Shaker M (2023) Synthesis, characterization, and biological activities of new conjugates of guanosine grafted on polyvinyl alcohol, carbohydrate chitosan, and cellulose. Polym Bull 80:6433–6454. https://doi.org/10.1007/s00289-022-04363-3
30. Schanté CE, Zuber G, Herlin C, Vandamme TF (2011) Chemical modifications of hyaluronic acid for the synthesis of derivatives for a broad range of biomedical applications. Carbohydr Polym 85:469–489. https://doi.org/10.1016/j.carbpol.2011.03.019
31. Hu L, Wang S, Shang L, Teng Y, Li J, Li B (2020) A novel strategy to maintain the long-term viscosity stability of konjac glucomannan hydrosol by using zinc ion. Int J Biol Macromol 151:106000. https://doi.org/10.1016/j.ijbiomac.2020.106000

32. Kaczmarska K, Śmietana M, Drożyński D, Bobrowski A, Woźniak F (2024) Characterisation of polacrylate-polysacharide system. Part I. Infrared structural studies. J Cast Mater Eng 8:11–18. https://doi.org/10.7494/jcme.2024.8.1.11
33. Nissola C, Marchioro MLK, Mello EVSL, Guidi AC, Medeiros DC, da Silva CG, Palazzo de Mello JC, Pereira EA, Barbosa-Dekker AM, Dekker RFH, Cunha MAA (2021) Hydrogel containing (1 → 6)-β-D-glucan (lasiodiplodan) effectively promotes dermal wound healing. Int J Biol Macromol 183:316–330. https://doi.org/10.1016/j.ijbiomac.2021.04.169
34. Alvarez X, Alves A, Ribeiro MP, Lazzari M, Coutinho P, Otero A (2021) Biochemical characterization of Nostoc sp. exopolysaccharides and evaluation of potential use in wound healing. Carbohydr Polym 254:117303. https://doi.org/10.1016/j.carbpol.2020.117303
35. Li W, Fang K, Yuan H, Li D, Li H, Chen Y, Luo X, Zhang L, Ye X (2023) Acid-induced Poria cocos alkali-soluble polysaccharide hydrogel: Gelation behaviour, characteristics, and potential application in drug delivery. Int J Biol Macromol 242:124383. https://doi.org/10.1016/j.ijbiomac.2023.124383
36. Xue X, Song G, Chang C (2022) Tough all-polysaccharide hydrogels with uniaxially/planarly oriented structure. Carbohydr Polym 288:119376. https://doi.org/10.1016/j.carbpol.2022.119376
37. Zhang P, Sun Y, Yang H, Liu D, Zhang F, Zhang Y, Zhong W, Zuo B, Zhou Z (2023) Vancomycin-loaded silk fibroin microspheres in an injectable hydrogel for chronic osteomyelitis therapy. Front Bioeng Biotechnol 11:1163933. https://doi.org/10.3389/fbioe.2023.1163933
38. Daaboul M, Hancer H, Ozbek T, Su E, Topuzogullari M, Özmen MM (2025) Multifunctional quaternized 4-vinylpyridine-based cryogels: A synthetic cationic platform for dye adsorption and antibacterial performance. Eur Polym J 236:114131. https://doi.org/10.1016/j.eurpolymj.2025.114131
39. Pacelli S, Di Muzio L, Paolicelli P, Fortunati V, Petralito S, Trilli J, Casadei MA (2021) Dextran-polyethylene glycol cryogels as spongy scaffolds for drug delivery. Int J Biol Macromol 166:1292–1300. https://doi.org/10.1016/j.ijbiomac.2020.10.273
40. Alves P, Simão AF, Graça MFP, Mariz MJ, Correia IJ, Ferreira P (2023) Dextran-based injectable hydrogel composites for bone regeneration. Polymers 15:4501. https://doi.org/10.3390/polym15234501
41. Radhouani H, Bicho DF, Gonçalves C, Maia FR, Reis RL, Oliveira JM (2019) Kefiran cryogels as potential scaffolds for drug delivery and tissue engineering applications. Mater Today Commun 20:100554. https://doi.org/10.1016/j.mtcomm.2019.100554
42. Radhouani H, Gonçalves C, Maia FR, Oliveira EP, Reis RL, Oliveira JM (2023) Development of conjugated kefiran-chondroitin sulphate cryogels with enhanced properties for biomedical applications. Pharmaceutics 15:1662. https://doi.org/10.3390/pharmaceutics15061662
43. Şeker Ş, Elçin AE, Elçin YM (2020) Macroporous elastic cryogels based on platelet lysate and oxidized dextran as tissue engineering scaffold: In vitro and in vivo evaluations. Mater Sci Eng C 110:110703. https://doi.org/10.1016/j.msec.2020.110703
44. Yin N, Stilwell MD, Santos TMA, Wang H, Weibel DB (2015) Agarose particle-templated porous bacterial cellulose and its application in cartilage growth in vitro. Acta Biomater 12:129–138. https://doi.org/10.1016/j.actbio.2014.10.019
45. Concórdio-Reis P, Martins M, Araújo D, Alves VD, Moppert X, Guézennec J, Reis MAM, Freitas F (2024) Iron(III) cross-linked hydrogels based on *Alteromonas macleodii* Mo 169 exopolysaccharide. Int J Biol Macromol 274:133312. https://doi.org/10.1016/j.ijbiomac.2024.133312
46. Liao CH, Chen CS, Chen YC, Jiang NE, Farn CJ, Shen YS, Hsu ML, Chang CH (2020) Vancomycin-loaded oxidized hyaluronic acid and adipic acid dihydrazide hydrogel: Bio-compatibility, drug release, antimicrobial activity, and biofilm model. J Microbiol Immunol Infect 53:525–531. https://doi.org/10.1016/j.jmii.2019.08.008
47. Betancourt-Galindo R, Cárdenas-Valdés X, Sánchez-Orozco JL, Ledezma A, Puente-Urbina B, Meléndez-Ortiz HI (2025) Synthesis of copolymer hydrogels based on maltodextrin and chitosan with antimicrobial properties for their potential use as wound dressings. Int J Biol Macromol 323:147140. https://doi.org/10.1016/j.ijbiomac.2025.147140

Publisher's note Springer Nature remains neutral with regard to jurisdictional claims in published maps and institutional affiliations.

Authors and Affiliations

Sanem Bulut[1] · Semra Tasdurmazli[2] · Esra Bedir[2] · Tulin Ozbek[2] · Esra Su[3] · Kader Korkmaz Edis[4] · Enes Dertli[5] · Mehmet Murat Ozmen[1]

✉ Mehmet Murat Ozmen
ozmenm@yildiz.edu.tr

1 Faculty of Chemical and Metallurgical Engineering, Department of Bioengineering, Yildiz Technical University, Istanbul 34220, Turkey

2 Faculty of Arts and Science, Department of Molecular Biology and Genetics, Yildiz Technical University, Istanbul 34220, Turkey

3 Faculty of Aquatic Sciences, Aquatic Biotechnology, Istanbul University, Istanbul 34134, Turkey

4 Faculty of Chemical and Metallurgical Engineering, Department of Food Engineering, Yildiz Technical University, Istanbul 34220, Turkey

5 Faculty of Chemical-Metallurgical Engineering, Department of Food Engineering, Istanbul Technical University, Istanbul 34467, Turkey